GDCh Research Article Angewandte International Edition Chemie www.angewandte.org

How to cite: *Angew. Chem. Int. Ed.* **2025**, *64*, e202501011
doi.org/10.1002/anie.202501011

Circularly Polarized Phosphorescence

Chiral Luminescent Ion Pair (CLIP) Strategy Enables Amorphous Platinum Complexes Circularly Polarized Phosphorescence

Sheng-Qi Qiu[+], Mei-Yuan Li[+], Hua-Yue Li, Yao Xiao, Jiannan Xiao, Gayathri Parthasarathy, Zhengong Meng, Wai-Yeung Wong, and Zhen-Qiang Yu**

Abstract: Chiral ion-pairing (CIP) has been developed as an effective chirality transfer strategy from chiral ionic species to its achiral counter-ionic substrate. When the achiral counter-ions were endowed with luminescent properties, the resultant chiral luminescent ion pair (CLIP) will open a new window for high-performance chiral luminescence. In this research, three pairs of CLIP molecules featuring the platinum complexes as achiral cationic luminophores and the chiral anion (CA) as chiral source were constructed. The CLIP molecules demonstrate circularly polarized phosphorescence (CPP) with quantum yields (Φ_{PL}) up to 71.5%, dissymmetry factor (g_{cpp}) values of 1.8×10^{-2} in amorphous state and g_{cpp} up to −0.99 in cholesteric liquid crystal (CLC). Results show that the chiroptical properties can be assigned to the chirality transfer from the CAs to the formed twisted dimeric or oligomeric self-assemblies of platinum complex cations. This research presents a new approach for achieving high-performance chiral luminescence of amorphous chiral metal complexes, providing a concise model for revealing the chirality transfer in CLIP materials.

Introduction

Chiral ion-pairing (CIP) is an effective chirality transfer strategy to transfer chirality from an enantiomerically pure ionic species to its achiral counter-ionic substrate or intermediate in asymmetric synthesis (Figure 1a).[1–3] When the achiral counter-ions were endowed with luminescent properties, the resultant chiral luminescent ion pair (CLIP) will open a new window for high-performance chiral luminescence. In the CLIP materials, the chiral anion (CA)/cation can transfer chirality to the achiral cationic/anionic luminophores via noncovalent interaction.[4] After the first report of a 2D Zn(II) metal-organic framework (MOF),[5] the CA strategy has been preliminarily applied to chiroptical materials such as small-molecular metal complexes,[6–8] coordination supramolecular assemblies,[9,10] and metal clusters,[11,12] representing a promising candidate for a wide range of optoelectronic applications. In this context, Zhong's group developed a series of diastereomeric mixtures composed of a chiral camphorsulfonate anion and a racemate of Ru or Ir complex cations.[6,7] The chiral electroluminescence property was greatly improved by addition of the chiral ionic liquid. Subsequently, You's group also reported a coassembly system constructed from achiral square-planar Pt(II) complex cations and chiral carboxylic anions.[8] Generally, the chiral ions and the achiral luminescent counter ions coassembled to form crystals or highly ordered assemblies with chiral luminescence. Though the chiral luminescence can be assigned to the chiral assembly of the achiral luminophores or the apparent presence of diastereoisomeric mixtures, there is a lack of a concise model to reveal the chirality transfer in CLIP materials.[12–15]

Due to the widespread applications in optoelectronic devices,[16] 3D display,[17] asymmetric synthesis,[18] information encryption,[19] and anticounterfeiting,[20] circularly polarized light received an increasing attention. The traditional device for obtaining circularly polarized light requires a linear polarizer and a quarter-wave plate. Circularly polarized luminescence (CPL) materials directly emit circularly polarized light, thus can simplify the optical devices and improve energy utilization efficiency. Therefore, the research on CPL has become a hot topic in the field of

[*] S.-Q. Qiu[+], M.-Y. Li[+], H.-Y. Li, Y. Xiao, J. Xiao, G. Parthasarathy, Z. Meng, Z.-Q. Yu
College of Chemistry and Environmental Engineering, Shenzhen University, Shenzhen 518060, China
E-mail: zqyu@szu.edu.cn

Z. Meng
Key Laboratory of Flexible Electronics & Institute of Advanced Materials, Nanjing Tech University, Nanjing 211816, China

Z. Meng, W.-Y. Wong
Department of Applied Biology and Chemical Technology and Research Institute for Smart Energy, The Hong Kong Polytechnic University, Hong Kong 999077, China
E-mail: wai-yeung.wong@polyu.edu.hk

W.-Y. Wong
The Hong Kong Polytechnic University Shenzhen Research Institute, Shenzhen 518057, China

[+] Both authors contributed equally to this work.

Additional supporting information can be found online in the Supporting Information section

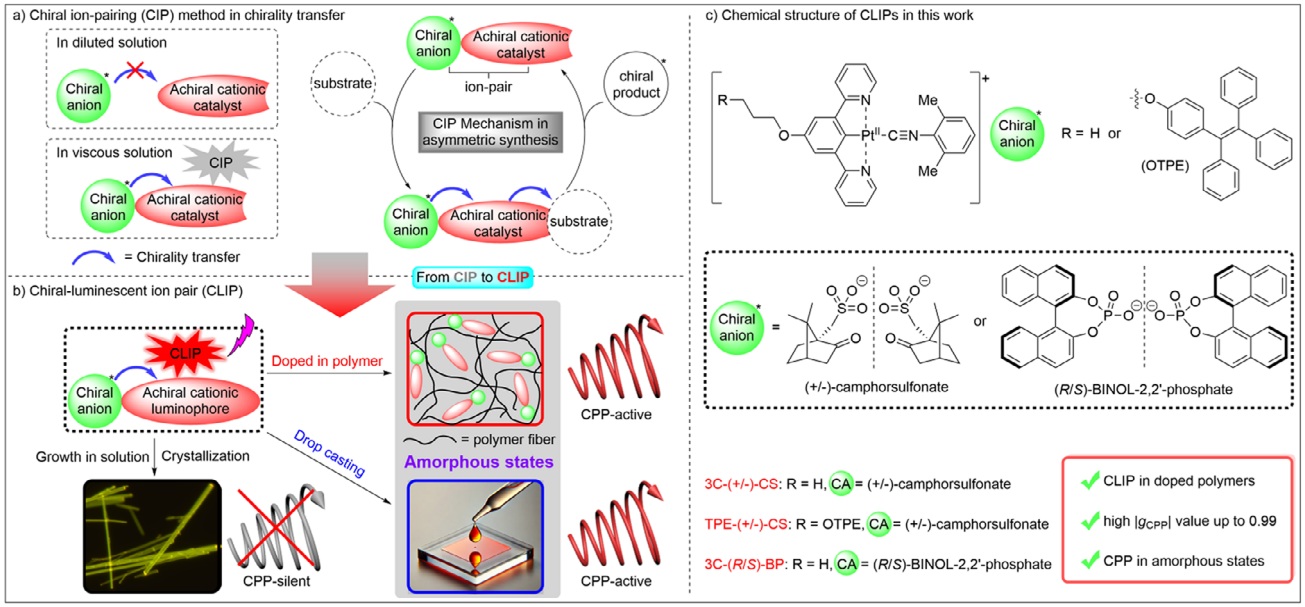

Figure 1. a) CIP method in chirality transfer. In classical asymmetric catalysis reaction with the CIP method, chirality was transferred from the chiral anion to the achiral counter cationic catalyst and further transferred to the reaction product. b) CLIP strategy that was applied in this work. CLIP materials in this work performed significant CPL activity in doped polymers and drop-cast films but became CPL-silent in well-organized nanorods. c) The specific structures of CLIP molecules in this work.

optoelectronics. The molecular design of CPL molecules generally involves connecting luminescent groups directly or through a certain length of the spacer to chiral groups. In most cases, CPL is achieved through direct excitation of chiral luminescent molecules or their assemblies,[21–23] or through simultaneous chirality and energy transfer.[24,25] Considering the rich structural controllability and excellent phosphorescence performance,[26,27] introducing CAs into small-molecular metal complexes may endow the materials with high-performance circularly polarized phosphorescence (CPP) properties.

The morphology of CPL materials plays a crucial role in their chiroptical properties. The luminescence dissymmetry factor (g_{lum}) could be amplified through supramolecular assembly[8,28] or crystal engineering,[11,29] thus far exceeding the g_{lum} value in their amorphous states. Despite the superior performance in CPL, crystalline or supramolecularly assembled chiral small-molecular metal complexes usually suffered from poor processability or harsh preparation conditions and seriously limited their applications. On the contrary, amorphous materials can compensate for the poor processability and stringent preparation conditions, but in most cases, the disordered molecular arrangement can seriously reduce their chiroptical properties.[6,7,30] Thus, realizing high-performance CPP properties of chiral small-molecular metal complexes in amorphous state is urgently needed.

Here, three pairs of CLIP molecules composed of achiral luminescent platinum cations and CAs were synthesized. The samples with different morphologies exhibit different chirality transfer behaviors, which resulted in high-performance CPP in doped polymer (Figure 1b, right top) and drop-cast film (Figure 1b, right bottom), but poor CPP or even no CPP activity was observed in well-organized nanorods (Figure 1b, left bottom). The specific structures of CLIP molecules 3C-(±)-CS, TPE-(±)-CS, and 3C-(*R*/*S*)-BP were shown in Figure 1c, and the achiral cationic platinum complexes exhibited high-performance CPP from yellow to red region in amorphous state.

Results and Discussion

After synthesizing the corresponding N^C^N pincer ligands and chelating them with potassium tetrachloroplatinate, the CLIP molecules were synthesized by introducing 2,6-dimethylphenylisocyanide and CAs (±)-camphorsulfonate ((±)-CS) or (*R*/*S*)-BINOL-2,2′-phosphate ((*R*/*S*)-BP) into the square-planar platinum complexes (see Supporting information). The chemical structures were confirmed by ^{1}H, ^{13}C, and ^{31}P nuclear magnetic resonance spectroscopy (Figures S1–S26), and high-resolution mass spectrometry (Figures S27–S38). The photophysical behaviors were investigated by UV–vis absorption, photoluminescence (PL), circular dichroism (CD), and CPL. The presence of nanorods was confirmed by field-emission scanning electron microscope (FE-SEM). The wide-angle X-ray diffraction (WAXD) was applied to investigate the morphology of drop-cast film and doped polymers. Despite multiple efforts, we were still not able to purify the material TPE-(*R*/*S*)-BP due to the similar solubilities of the impurities.

Due to the similar property between enantiomers, 3C-(−)-CS, 3C-(*R*)-BP, and TPE-(−)-CS were chosen to investigate their photophysical properties in DCM solutions, doped PMMA films, and drop-cast films. As the dotted black lines shown in Figure 2a,c,e, the absorption in DCM between 380 and 480 nm can be assigned to the low-energy metal-to-ligand

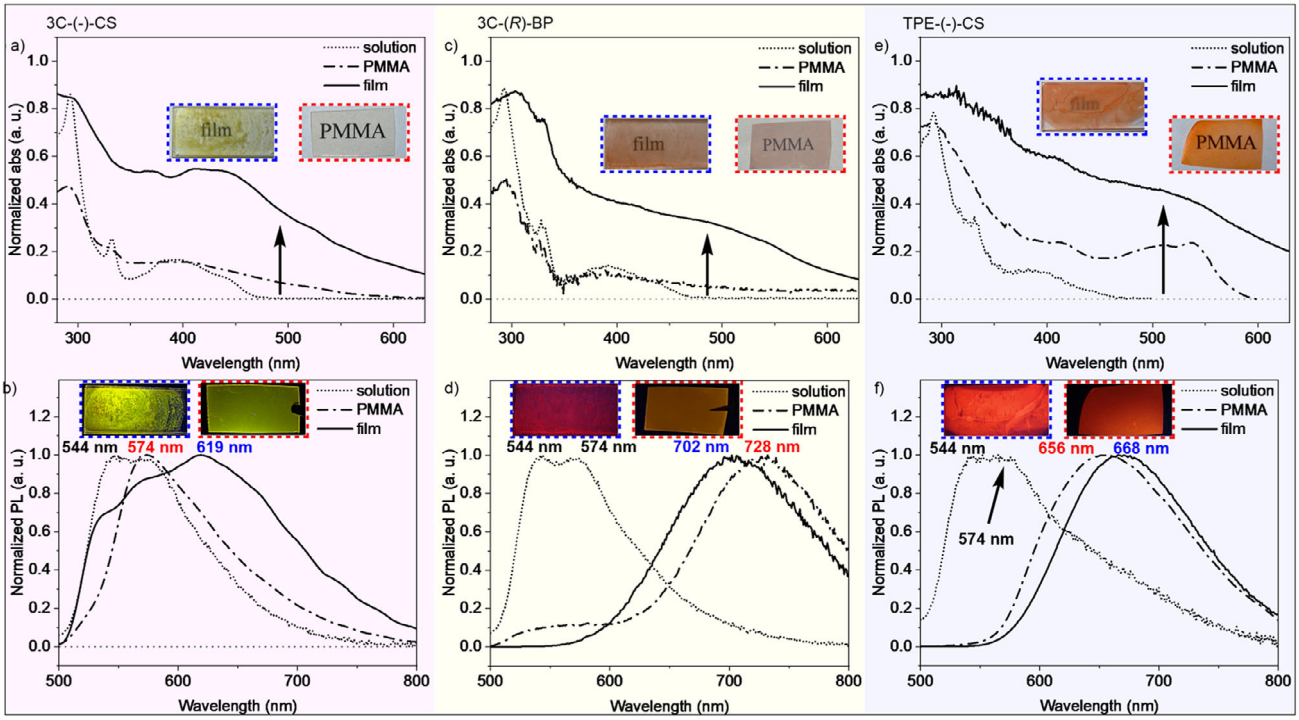

Figure 2. a), c), and e), Absorption spectra of 3C-(−)-CS, 3C-(*R*)-BP, and TPE-(−)-CS under daylight in DCM, in doped PMMA or in drop-cast film. Insets are the corresponding photos under daylight. b), d), and e), Luminescence spectra of 3C-(−)-CS, 3C-(*R*)-BP, and TPE-(−)-CS in DCM, in doped PMMA, or in drop-cast film excited at 395, 405, and 385 nm, respectively. Insets are the corresponding photos irradiated under UV 365 nm.

Table 1: Summary of the photophysical properties of the platinum complexes in DCM solution, PMMA, and drop-cast film.

Structure	$\lambda_{abs,max}$ (nm)[a] (solution)	λ_{Em} (nm) (PMMA)	τ (μs)[b] (PMMA)	PLQY (%) (PMMA)	λ_{Em} (nm) (film)	τ (μs)[b] (film)	PLQY (%) (film)
3C-(−)-CS	395	573	12.1	36.7	537/573/620	0.26	11.6
3C-(+)-CS	395	574	11.9	25.7	531/574/618	0.25	8.9
3C-(*R*)-BP	405	728	4.3	23.8	703	0.44	43.6
3C-(*S*)-BP	405	711	5.0	15.3	700	0.46	59.9
TPE-(−)-CS	385	645	3.0	39.6	680	0.42	63.1
TPE-(+)-CS	385	655	3.3	35.4	670	0.51	71.5

[a] The samples were dissolved in DCM with the concentration of 1×10^{-5} M. [b] Measured at the maximum emission wavelength.

charge-transfer (^{1}MLCT) absorption edge of known N^C^N monoplatinum complexes.[31] While in doped PMMA films (red lines in Figure 2a,c,e), the absorption wavelengths were redshifted to 500–600 nm, which could be attributed to singlet and triplet metal-metal-to-ligand charge-transfer (^{1}MMLCT and ^{3}MMLCT) absorptions of the cation–cation self-assembly via delocalization of $5d_z^2$(Pt) orbitals.[8,32] The absorption peaks were further expanded to above 650 nm in drop-cast films (solid blue lines in Figure 2a,c,e), indicating that the platinum cations involved in the self-assembly have larger size than that in doped PMMA films.

All the emission spectra in dilute solution (1×10^{-5} M in DCM) exhibited similar shape with two emissions peaked at 544 and 574 nm (dotted black lines in Figure 2b,d,f), relating to the usual MLCT emission and dimeric emission, respectively.[33] As the concentration increased, the emission of 3C-(−)-CS and TPE-(−)-CS changed little (Figures S41 and S43). Interestingly, the major emission peak of 3C-(*R*)-BP was redshifted to 574 nm (1×10^{-4} M DCM) and 635 nm (1×10^{-3} M DCM) (Figure S42), suggesting the improved Pt–Pt interaction and possible cation–π interaction. The emission peak of 3C-(−)-CS was redshifted to 574 nm when dispersed in PMMA (Figure 2b, chain red line), and further redshifted to 619 nm with two shoulders at 544 and 574 nm in drop-cast film (Figure 2b, solid blue line). These redshifts may be resulted from the dimeric assembly when dispersed in PMMA and Pt-Pt directed self-assembly in drop-cast film.[34] In contrast, 3C-(*R*)-BP exhibited a broad emission of a wavelength maximum at 728 and 702 nm in doped PMMA film (Figure 2d, red line) and in drop-cast film (Figure 2d, solid blue line), respectively. Compared with that of 3C-(−)-CS, the large redshift of 3C-(*R*)-BP can be attributed to the additional cation–π interaction between naphthalene rings of phosphate anions and the platinum complex cations. Notably, in the doped PMMA film of 3C-(*R*)-BP, a weak emission band was observed in the wavelength range of 500 and 600 nm,

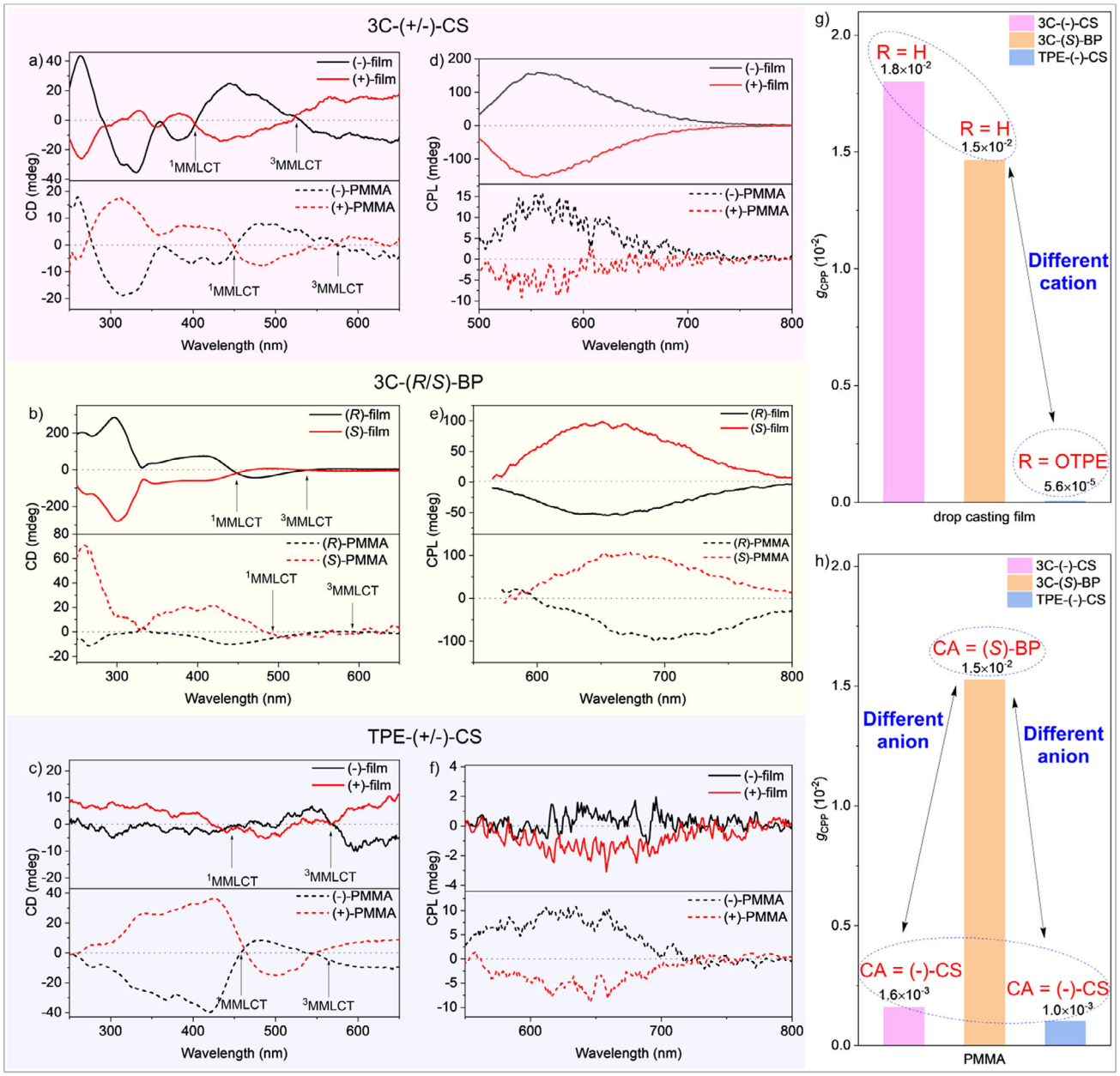

Figure 3. a–c) CD spectra of 3C-(±)-CS, 3C-(R/S)-BP, and TPE-(±)-CS in drop-cast films and doped PMMA films. d–f) CPL spectra of 3C-(±)-CS, 3C-(*R*/*S*)-BP, and 3C-(±)-CS in drop-cast films and doped PMMA films excited at 395, 405, and 385 nm, respectively. g) Comparison of the g_{CPP} values of 3C-(−)-CS (purple), 3C-(*S*)-BP (orange), and TPE-(−)-CS (blue) in drop-cast films, showing the similar g_{CPP} value between 3C-(−)-CS and 3C-(*S*)-BP with the same achiral cation. h) Comparison of the g_{CPP} values of 3C-(−)-CS (purple), 3C-(*S*)-BP (orange), and TPE-(−)-CS (blue) in doped PMMA films, showing similar g_{CPP} values between 3C-(−)-CS and TPE-(−)-CS with the same chiral anion.

suggesting the presence of dimeric molecular stacking, which is similar to that of 3C-(−)-CS. The interaction between cationic platinum and aromatic rings could be proved by the emission of TPE-(−)-CS. It was observed that isolated TPE group emitted at 441 nm in 1×10^{-5} DCM solution, but the emission gradually disappeared when the concentration increased (Figure S44), indicating the intermolecular energy transfer from the TPE group to the adjacent N^C^N-Pt cations. In doped PMMA film (Figure 2f, red line) and drop-cast film (Figure 2f, solid blue line), the emission peaks were redshifted to 656 and 668 nm, respectively. The above mentioned differences between solutions and films jointly revealed the dimeric or oligomeric assemblies of N^C^N-platinum cations in doped PMMA film and drop-cast films.

The photophysical properties of the complexes in amorphous states were summarized in Table 1. The doped PMMA films showed photoluminescence quantum yields (PLQYs) of 15.3%–39.6% with the decay lifetimes (τ) of 3.0–12.1 μs (Figure S39); while the drop-cast films exhibited PLQYs of 8.9%–71.5% with τ of 0.25–0.51 μs (Figure S40). Obviously, the overall lifetime in doped PMMA is much longer than that in drop-cast films. In PMMA, the luminescent complexes were

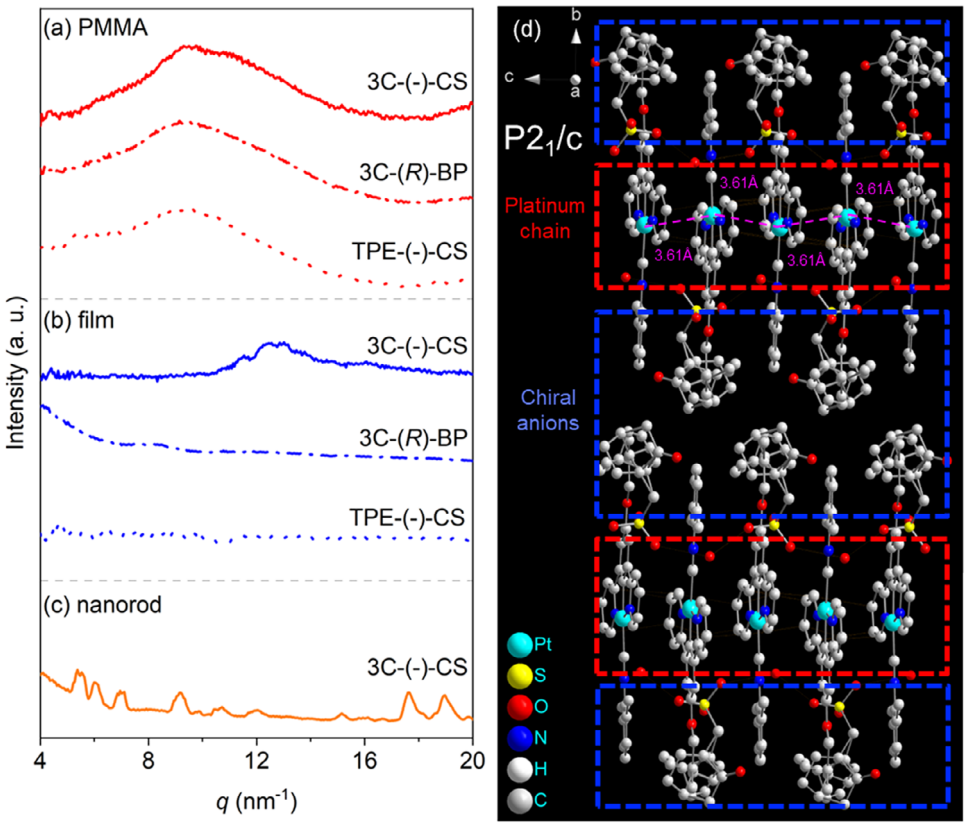

Figure 4. a) and b), WAXD patterns of 3C-(−)-CS, 3C-(*R*)-BP, and TPE-(−)-CS in doped PMMA films and drop-cast films, respectively. c) WAXD pattern of 3C-(−)-CS nanorod developed in DCM solution. d) Molecular packing of 3C-(−)-CS nanorod (all hydrogen atoms have been removed for clarity), showing achiral molecular packing of platinum cations dominated by Pt–Pt-directed self-assembly.

highly dispersed and the molecular motions were suppressed by the entanglement of macromolecular chains. When excited, the energy decay of the excited species was reduced by suppressing their molecular motions and intermolecular collision, thus leading to the lifetime extension.[35,36]

No circular dichroism (CD) signals of the three pairs of Pt complexes were detected in DCM solutions (Figure S45–S47), though 3C-(*R*/*S*)-BP showed CD signal of the chiral absorption of (*R*/*S*)-BP in DCM solution (Figure S46) between 250 and 300 nm (Figure S48). No CPL signals were observed in DCM solutions for all compounds (Figures S49–S51). The inactive CD or CPL in solutions could be attributed to significant solvation effects, which hindered the formation of CLIP in solutions and impeded the chirality transfer.

Different from the chiroptical behaviors in solutions, obvious CD and CPL signals were observed in doped PMMA films and drop-cast films (Figures 3a–f and S52–S63) except for TPE-(±)-CS in the drop-cast films. In doped PMMA films, both 3C-(−)-CS and TPE-(−)-CS displayed similar negative Cotton effects in the ^{3}MMLCT transition bands and positive Cotton effects in the ^{1}MMLCT transition bands, as shown in Figure 3a,c (black dashed lines), respectively; while 3C-(+)-CS and TPE-(+)-CS exhibited contrary Cotton effects in the same wavelength region (red dashed lines in Figure 3a,c, respectively). However, in drop-cast films, the CD signals of TPE-(±)-CS (Figure 3c, solid lines) were much poorer than those of 3C-(±)-CS (Figure 3a, solid lines), suggesting the twisted TPE group can destroy the chiral assembly and result in the poor CD signals. As for 3C-(*R*)-BP in drop-cast film, a negative Cotton effect in the ^{1}MMLCT transition band and a minor positive Cotton effects in the ^{3}MMLCT transition band were observed (Figure 3b, black solid lines); while for 3C-(*S*)-BP in doped PMMA films, a symmetric CD signal (Figure 3b, red solid lines) was detected. It should be noted that 3C-(*R*/*S*)-BP displayed only trace CD signals in the ^{3}MMLCT transition band, but evident CD signals in the ^{1}MMLCT transition band (Figure 3b, dashed lines). The trace CD signals in the ^{3}MMLCT transition band, combined with the larger emission redshift relative to 3C-(±)-CS (Figure 2b), suggest a different assembly behavior of 3C-(*R*/*S*)-BP from that of 3C-(±)-CS, probably due to a tight integration between N^C^N-platinum cation and BP anion through cation–π interaction, and thus the formation of CLIP.

All the samples, whether in drop-cast films or in doped PMMA films, exhibited mirror symmetric CPPs at their emission wavelength regions (Figure 3d–f). As summarized in Figure 3g, the g_{CPP} values of 3C-(−)-CS, 3C-(*S*)-BP, and TPE-(−)-CS at the maximum emission wavelength in drop-cast films were 1.8×10^{-2}, 1.5×10^{-2}, and 5.6×10^{-5}, respectively; while the corresponding g_{CPP} values in doped PMMA films were 1.6×10^{-3}, 1.5×10^{-2}, and 1.0×10^{-3}, as shown in Figure 3h. Samples with enantiomeric anions exhibited the symmetric CPP behaviors (Figures S73–S74).

Interestingly, with the same CA, 3C-(±)-CS and TPE-(±)-CS exhibited significant difference in g_{CPP} values in drop-cast films (Figure 3g, purple columns vs. blue columns), while the g_{CPP} values in their doped PMMA films were almost identical (Figure 3h, purple columns vs. blue columns). At the same time, with the same N^C^N-platinum cation, 3C-(±)-CS exhibited similar g_{CPP} values as that of 3C-(*R*/*S*)-BP in drop-cast films (Figure 3g, purple columns vs. orange columns), but different in the order of magnitude in doped PMMA films (Figure 3h, purple columns vs. orange columns). Hence, it indicated that the CPP behavior in drop-cast films was determined by the cationic species, while in doped PMMA films, it was mainly determined by the CA species. This also will be discussed in the discussion section.

To gain a deep insight into the chirality transfer mechanism behind the CPP behaviors, WAXD experiments were carried out to explore the morphology in drop-cast film and in PMMA-doped film. Interestingly, all drop-cast films and doped PMMA films only exhibited an amorphous halo and no sharp reflection in the wide-angle region (Figure 4a,b), indicating that no crystalline or highly ordered structure was formed. To the best of our knowledge, nearly all of the reported CPP materials based on CA strategy perform better chiroptical properties in well-organized states, such as microcrystals[6–8] or microwires,[23] but nearly chiroptical-inactive in amorphous states. Thus, the 3C-(−)-CS nanorods were also prepared in methanol and measured by WAXD (Figure 4c) and FE-SEM (Figures S64 and S65). The assemblies of 3C-(−)-CS showcased elongated structures even up to millimeters in length. As expected, the nanorods exhibited yellow emission under fluorescence microscope (Figure S66), but no CD and CPP signals were detected (Figures S67–S70). As shown in Figure 4d, the assembled model of the nanorod belongs to $P2_1/c$ space group determined by X-ray crystallographic analysis (CCDC 2410662).[37] The cations stacked in a symmetric face-to-tail fashion and formed a 1D platinum chain with the distance of adjacent platinum atoms being 3.607 Å, and the CAs were excluded from the platinum chain, indicating the Pt–Pt-directed self-assembly was the dominant interaction during the nanorod growth, which resulted in the achiral luminescent property.

Based on the above discussion, the proposed mechanisms of CPP generation in amorphous states were established and illustrated in Figure 5. In solution, due to the solvated effect, the distance between the platinum cations or CAs was greatly increased and thus the chirality of CAs cannot be transferred to the achiral platinum cations. When dispersed in PMMA, N^C^N-platinum cations formed dimers due to the strong Pt–Pt interaction and polymer entanglement, and the negative CAs located in the vicinity of the positive platinum centers formed CLIPs through ionic bonding and thus forming CLIPs. Due to the short distance between the CA and the luminescent part, the chirality of CAs was effectively transferred to the cationic dimers, thus the twisted assembly emitted CPP (Figure 5, left). Due to the possible cation–π interaction between the N^C^N pincer ligands and the BP anions, the BP anions (g_{CPP} of 10^{-2}) exhibit a better chirality transfer effect than that of CS anions (g_{CPP} of 10^{-3}). To exclude the observed CPP properties ascribed

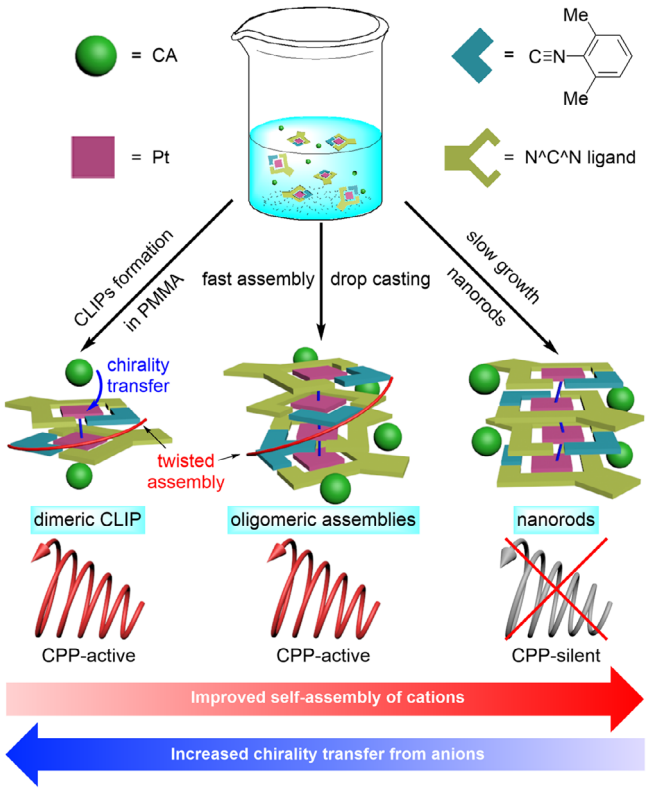

Figure 5. In doped PMMA films, the cationic platinum complexes were dispersed and formed twisted dimeric CLIP by polymer chains. In drop-cast films, the cationic platinum complexes fast assembled into oligomeric assemblies due to the rapid solvent evaporation and formed oligomeric CLIP. In crystal or highly ordered assemblies, the cationic platinum complexes formed platinum chains and the CAs were completely excluded from the platinum chains and destroyed the CLIP formation. There is a slight angle between the phenyl ring of the iso-nitrile ligand and the N^C^N-Pt plane. With the improvement of the self-assembly of cations, the direct chirality transfer from CA to achiral cation was decreased.

directly to PMMA, control experiments were conducted by CPL measurements (Figure S76). As for the materials of drop-cast film, the N^C^N-platinum cations and the CAs disorderly aggregated during the rapid evaporation of solvent. In this case, the aggregation rate of N^C^N-platinum cations was too fast to form long-range ordered self-assembled structure, while only amorphous metastable oligomers were formed (Figure 5, middle). The chiral-anion-disturbed twisted assemblies were proved by DFT calculations (see Supporting Information). The IR spectra suggested that chiral anions exhibited as noncoordinated anions in the amorphous states (Figure S77). With a twisted TPE group attached to the N^C^N pincer, the metastable oligomeric assembly was disrupted, the distance between the CAs and the platinum cations greatly increased and no CLIP was formed, resulting in the much lower g_{CPP} (g_{CPP} of 10^{-5}) than that of 3C-(±)-CS and 3C-(*R*/*S*)-BP (g_{CPP} of 10^{-2}) in drop-cast films. In brief, with the self-assembly of platinum cations improved, the CAs were gradually excluded from the platinum chain, resulting in the decreased chirality transfer from CAs to luminescent cations. In the amorphous state of doped PMMA

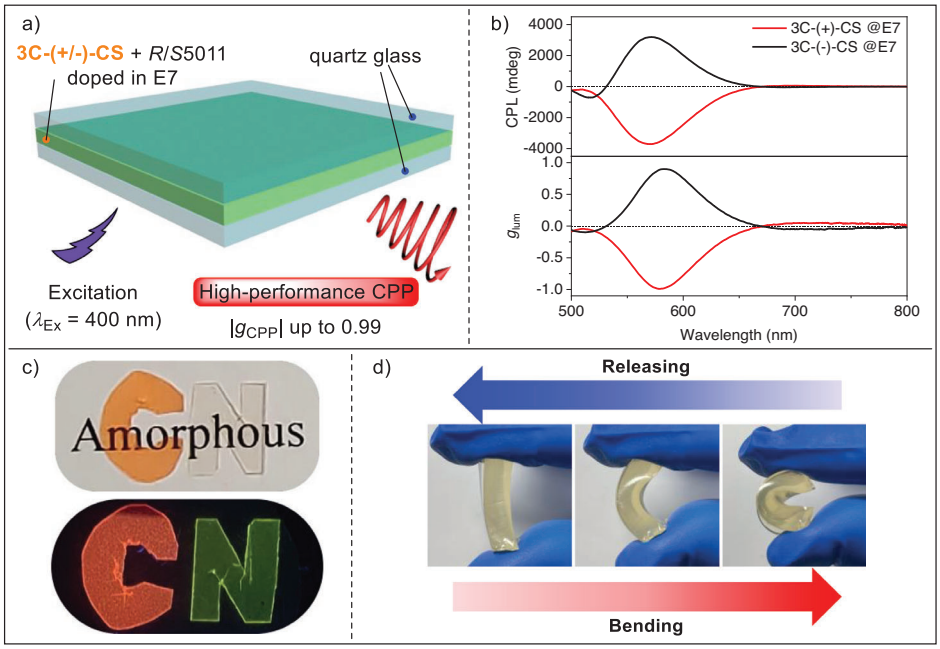

Figure 6. a) Structural diagram of simple CPP device. 3C-(±)-CS was doped in the prepared CLC (2.4 wt% of *S*/*R*5011 doped in E7) and sealed in quartz glass liquid crystal cells. b) CPL spectra of simple CPP devices excited at 395 nm. c) Collage pattern of doped PMMA films under daylight and UV (365 nm). The letter C was made of TPE-(+)-CS-doped PMMA film and the letter N was made of 3C-(−)-CS-doped PMMA film. d) Elastic deformation of the doped PDMS block of 3C-(*S*)-BP.

or drop-cast film, the CAs could disturb the Pt–Pt-directed self-assembly process of platinum cations, thus giving rise to a significant chiroptical performance even in the twisted self-assembly. As an extreme example, the slowly grown nanorods (Figure 5, right) from dilute solution completely avoid the disturbance of the CAs and form a highly symmetric assembly with a achiral space group, thus exhibiting no chiral characteristics.

To further demonstrate the good processability and the diversified application scenarios of the amorphous CLIP materials, a pair of simple CPP devices of 3C-(±)-CS (Figure 6a,b, for preparation details, see Supporting Information) was prepared. As shown in Figure 6a, 3C-(±)-CS was doped in room temperature cholesteric liquid crystal (CLC) (2.4 wt% of *S*/*R*5011 doped in E7) and sealed in quartz glass liquid crystal cells to form the simple CPP device. The photonic bandgap wavelength of the CLC was adjusted to the range of 500–650 nm to fit the emission of 3C-(±)-CS (Figure S71). The simple device exhibited high-performance CPP with g_{CPP} values up to 0.90 and −0.99 for 3C-(−)-CS (Figure 6b, black lines) and 3C-(+)-CS (Figure 6b, red lines), respectively. The collage pattern of doped PMMA films (Figure 6c) and an elastomeric-doped polydimethylsiloxane (PDMS) material of 3C-(*S*)-BP (Figure 6d) were also prepared and investigated. The transparent doped PMMA films can be cut into small pieces with different shapes, indicating their amorphous morphology and good processability (Figure 6c). The doped PDMS material can be freely processed (Figure S72) and exhibits elastic deformation such as significant bending and rapid recovery (Figure 6d), manifesting excellent elasticity and processing performance. Furthermore, even in the doped PDMS block, 3C-(*S*)-BP can emit yellow CPP with g_{CPP} value near 10^{-2} (Figure S73) and PLQY of 2.5% under excitation of 400 nm light.

Conclusion

In summary, three pairs of CPP-active CLIP molecules were synthesized by introducing CAs to counter cationic Pt^{II} complexes. Although the crystal exhibited no CPP activity, the materials exhibited CPP emission with PLQY of up to 71.5% and g_{CPP} values of about 10^{-2} in amorphous states. By doping into CLC, the materials showed ultrahigh g_{CPP} up to −0.99. When the platinum cations formed crystalline or highly ordered structures through Pt–Pt-directed self-assembly, the chiral anions were excluded from the platinum chain and exhibited negligible influence on the platinum complexes, thus exhibiting no CPP activity. In the doped PMMA or drop-cast film, the platinum complexes formed amorphous dimers or oligomers due to the entanglement of the polymer chains or rapid solvent evaporation, and the chiral anions had significant influence on the platinum complexes, thus transferring chirality to the achiral platinum complex cations. By constructing CLIP molecules and utilizing polymer entanglement or rapid solvent evaporation to form amorphous structures, we have successfully solved the trade-off problem between low processability and high asymmetry factor.

Supporting Information

Synthetic procedures and data, experimental details, photophysical characterizations, and chiroptical properties.

The authors have cited additional references within the Supporting Information.[38–44]

Acknowledgements

This work was supported by the National Natural Science Foundation of China (Nos. 22272109, 21875143, and 52073242), the Guangdong Basic and Applied Basic Research Foundation (2024A1515011045), the Innovation Research Foundation of Shenzhen (Nos. JCYJ20220818095807016 and JCYJ20210324095406017), the RGC Senior Research Fellowship Scheme (SRFS2021-5S01), the Hong Kong Research Grants Council (PolyU 15301922), the CAS-Croucher Funding Scheme for Joint Laboratories (ZH4A), the Research Institute for Smart Energy (CDAQ), and Miss Clarea Au for the Endowed Professorship in Energy (847S). Special thanks goes to X.-Y. Chang and H.-H. Liu from the Southern University of Science and Technology for their assistance in crystal analysis. The authors also acknowledge the support from the Instrumental Analysis Center of Shenzhen University (Lihu Campus).

Conflict of Interests

The authors declare no conflict of interest.

Data Availability Statement

The data that support the findings of this study are available from the corresponding author upon reasonable request.

Keywords: Amorphous state · Chiral luminescent ion pair · Chirality transfer · Circularly polarized phosphorescence · Platinum complex

[1] J. M. Ovian, P. Vojáčková, E. N. Jacobsen, *Nature* **2023**, *616*, 84–89.
[2] S. Das, C. Zhu, D. Demirbas, E. Bill, C. K. De, B. List, *Science* **2023**, *379*, 494–499.
[3] A. Franchino, À. Martí, A. M. Echavarren, *J. Am. Chem. Soc.* **2022**, *144*, 3497–3509.
[4] Y.-Y. Zhao, Z.-Q. Li, Z.-L. Gong, S. Bernhard, Y.-W. Zhong, *Chem. Eur. J.* **2024**, *30*, e202400685.
[5] Y. Wen, T. Sheng, S. Hu, X. Ma, C. Tan, Y. Wang, Z. Sun, Z. Xue, X. Wu, *Chem. Commun.* **2013**, *49*, 10644.
[6] Z.-Q. Li, Y.-D. Wang, J.-Y. Shao, Z. Zhou, Z.-L. Gong, C. Zhang, J. Yao, Y.-W. Zhong, *Angew. Chem. Int. Ed.* **2023**, *62*, e202302160.
[7] Z.-Q. Li, Z.-L. Gong, T. Liang, S. Bernhard, Y.-W. Zhong, J. Yao, *Sci. China Chem.* **2023**, *66*, 2892–2902.
[8] G. Park, D. Y. Jeong, S. Y. Yu, J. J. Park, J. H. Kim, H. Yang, Y. You, *Angew. Chem. Int. Ed.* **2023**, *62*, e202309762.
[9] R.-J. Li, J. J. Holstein, W. G. Hiller, J. Andréasson, G. H. Clever, *J. Am. Chem. Soc.* **2019**, *141*, 2097–2103.
[10] Q. Bai, Y.-M. Guan, T. Wu, Y. Liu, Z. Zhai, Q. Long, Z. Jiang, P. Su, T.-Z. Xie, P. Wang, Z. Zhang, *Angew. Chem. Int. Ed.* **2023**, *62*, e202309027.
[11] J. Y. Wang, J. W. Yuan, X. M. Liu, Y. J. Liu, F. Bai, X. Y. Dong, S. Q. Zang, *Aggregate* **2024**, *5*, e508.
[12] K. Xiao, Y. Xue, B. Yang, L. Zhao, *CCS Chem* **2020**, *2*, 488–494.
[13] S. Yin, X. Li, H. Wang, J. Li, W. Huang, T. Gao, P. Yan, Y. Zhou, H. Li, *CrystEngComm* **2023**, *25*, 1541–1549.
[14] W. Chen, Z. Tian, Y. Li, Y. Jiang, M. Liu, P. Duan, *Chem. Eur. J.* **2018**, *24*, 17444–17448.
[15] W. Ye, Z. Meng, G. Zhan, A. Lv, Y. Gao, K. Shen, H. Ma, H. Shi, W. Yao, L. Wang, W. Huang, Z. An, *Adv. Mater.* **2024**, *36*, 2410073.
[16] D. Zhang, M. Li, C. F. Chen, *Chem. Soc. Rev.* **2020**, *49*, 1331–1343.
[17] Y. J. Zhou, Y. X. Wang, Y. H. Song, S. S. Zhao, M. J. Zhang, G. E. Li, Q. Guo, Z. Tong, Z. Y. Li, S. Jin, H. B. Yao, M. Z. Zhu, T. T. Zhuang, *Nat. Commun.* **2024**, *15*, 251.
[18] C. L. He, G. Yang, Y. Kuai, S. Z. Shan, L. Yang, J. G. Hu, D. G. Zhang, Q. J. Zhang, G. Zou, *Nat. Commun.* **2018**, *9*, 5117.
[19] S. Y. Lin, Y. Q. Tang, W. X. Kang, H. K. Bisoyi, J. B. Guo, Q. Li, *Nat. Commun.* **2023**, *14*, 3005.
[20] F. Nie, D. P. Yan, *Nat. Commun.* **2024**, *15*, 5519.
[21] C. Liu, J.-C. Yang, J. W. Y. Lam, H.-T. Feng, B. Z. Tang, *Chem. Sci.* **2022**, *13*, 611–632.
[22] L. Yuan, Y.-P. Zhang, Y.-X. Zheng, *Sci. China Chem.* **2024**, *67*, 1097–1116.
[23] Z.-L. Gong, T.-X. Dan, J.-C. Chen, Z.-Q. Li, J. Yao, Y.-W. Zhong, *Angew. Chem. Int. Ed.* **2024**, *63*, e202402882.
[24] Y.-J. Liu, Y. Liu, S.-Q. Zang, *Angew. Chem. Int. Ed.* **2023**, *62*, e202311572.
[25] Y. Wu, C. X. Yan, X. S. Li, L. H. You, Z. Q. Yu, X. F. Wu, Z. G. Zheng, G. F. Liu, Z. Q. Guo, H. Tian, W. H. Zhu, *Angew. Chem. Int. Ed.* **2021**, *60*, 24549–24557.
[26] J. Gong, X. Zhang, *Coord. Chem. Rev.* **2022**, *453*, 214329.
[27] X.-Y. Luo, M. Pan, *Coord. Chem. Rev.* **2022**, *468*, 214640.
[28] Y. Deng, M. Wang, Y. Zhuang, S. Liu, W. Huang, Q. Zhao, *Light Sci. Appl.* **2021**, *10*, 76.
[29] Z.-L. Gong, X. Zhu, Z. Zhou, S.-W. Zhang, D. Yang, B. Zhao, Y.-P. Zhang, J. Deng, Y. Cheng, Y.-X. Zheng, S.-Q. Zang, H. Kuang, P. Duan, M. Yuan, C.-F. Chen, Y. S. Zhao, Y.-W. Zhong, B. Z. Tang, M. Liu, *Sci. China Chem.* **2021**, *64*, 2060–2104.
[30] Y. Wang, D. Niu, G. Ouyang, M. Liu, *Nat. Commun.* **2022**, *13*, 1710.
[31] Z. Wang, E. Turner, V. Mahoney, S. Madakuni, T. Groy, J. Li, *Inorg. Chem.* **2010**, *49*, 11276–11286.
[32] Y.-C. Wei, S. F. Wang, Y. Hu, L.-S. Liao, D.-G. Chen, K.-H. Chang, C.-W. Wang, S.-H. Liu, W.-H. Chan, J.-L. Liao, W.-Y. Hung, T.-H. Wang, P.-T. Chen, H.-F. Hsu, Y. Chi, P.-T. Chou, *Nat. Photonics* **2020**, *14*, 570–577.
[33] S. J. Farley, D. L. Rochester, A. L. Thompson, J. A. K. Howard, J. A. G. Williams, *Inorg. Chem.* **2005**, *44*, 9690–9703.
[34] M. Chaaban, S. Lee, J. S. R. V. Winfred, X. Lin, B. Ma, *Small Struct.* **2022**, *3*, 2200043.
[35] S. Hirata, M. Vacha, *Adv. Opt. Mater.* **2017**, *5*, 1600996.
[36] M. Louis, H. Thomas, M. Gmelch, A. Haft, F. Fries, S. Reineke, *Adv. Mater.* **2019**, *31*, 1807887.
[37] Deposition Number 2410662 for 3C-(−)-CS contains the supplementary crystallographic data for this paper. These data are provided free of charge by the joint Cambridge Crystallographic Data Centre and Fachinformationszentrum Karlsruhe Access Structures service.
[38] Z.-L. Gong, Y.-W. Zhong, *Organometallics* **2013**, *32*, 7495–7502.
[39] B. Juršić, *Tetrahedron* **1988**, *44*, 6677–6680.
[40] P. Pander, A. V. Zaytsev, A. Sil, J. A. G. Williams, P.-H. Lanoe, V. N. Kozhevnikov, F. B. Dias, *J. Mater. Chem. C* **2021**, *9*, 10276–10287.
[41] L. Zeng, Y. Xiao, J. Jiang, H. Fang, Z. Ke, L. Chen, J. Zhang, *Inorg. Chem.* **2019**, *58*, 10019–10027.

[42] Q. Chen, D. Zhang, G. Zhang, X. Yang, Y. Feng, Q. Fan, D. Zhu, *Adv. Funct. Mater.* **2010**, *20*, 3244–3251.
[43] C. Po, C.-H. Tao, K.-F. Li, C. K. M. Chan, H. L.-K. Fu, N. Zhu, K.-W. Cheah, V. W.-W. Yam, *J. Organomet. Chem.* **2019**, *881*, 13–18.
[44] M. J. Frisch, G. W. Trucks, H. B. Schlegel, G. E. Scuseria, M. A. Robb, J. R. Cheeseman, G. Scalmani, V. Barone, G. A. Petersson, H. Nakatsuji, X. Li, M. Caricato, A. V. Marenich, J. Bloino, B. G. Janesko, R. Gomperts, B. Mennucci, H. P. Hratchian, J. V. Ortiz, A. F. Izmaylov, J. L. Sonnenberg, D. Williams-Young, F. Ding, F. Lipparini, F. Egidi, J. Goings, B. Peng, A. Petrone, T. Henderson, D. Ranasinghe, et al., Gaussian 16, Revision A.03, Gaussian, Inc., Wallingford, CT, **2016**.

Manuscript received: January 28, 2025
Revised manuscript received: April 10, 2025
Accepted manuscript online: April 12, 2025
Version of record online: April 21, 2025